Two-dimensional imaging of state-selected photofragments: the 355 nm photolysis of NO_2

T. Suzuki [1], V.P. Hradil, S.A. Hewitt [2], P.L. Houston
Department of Chemistry, Cornell University, Ithaca, NY 14853-1301, USA

and

B.J. Whitaker
School of Chemistry, Leeds University, Leeds LS1 9JT, UK

Received 26 August 1991

Two-dimensional photofragment imaging has been applied to the 355 nm photodissociation of NO_2 in a supersonic beam. The NO fragments are state-selectively ionized and projected onto a two-dimensional position-sensitive detector. The original velocity distribution is reconstructed by an Abel transform of the observed image of the fragments. The speed distribution of a single rovibrational state of NO consists of a single peak as expected from conservation of momentum and energy. The anisotropy parameter, β, of the NO photofragments is found to be 1.40 ± 0.20, which is significantly larger than previously reported values measured with effusive molecular beams. This discrepancy is explained by the effect of the rotation of the parent molecule.

1. Introduction

Two-dimensional imaging of state-selected photodissociation products detected by resonance-enhanced multiphoton ionization (REMPI) was first demonstrated in the 266 nm photodissociation of methyl iodide [1]. Briefly, this technique allows the experimenter to "map" the velocity distribution of the products in photodissociations and bimolecular reactions by directly imaging their spatial distribution onto a two-dimensional position-sensitive detector. The velocity (angle and speed) distribution of products in a single quantum state provides more detailed information about the reaction dynamics than previous Doppler [2], one-dimensional time-of-flight or "core-sampling" techniques [3,4], and conventional crossed beam experiments. One advantage of this method is simultaneous detection and characterization of competing (e.g. parallel and perpendicular) dissociation channels. Since its first demonstration, the method has been further applied to the 266 nm dissociation of methyl iodide [5,6] and the 243 nm dissociation of H_2S [7]. Recently the technique has also been applied to measurements of bond-dissociation energies [8] and reactive scattering [9]. The method is similar to the technique recently used to obtain the kinetic energy release in dissociative electron attachment of chlorofluorocarbons [10]. These approaches can be considered to be a quantitative variant of the photolysis mapping technique [11].

The photodissociation of NO_2 in the UV region has been studied by a number of researchers. It has been well established that the photoabsorption occurs mainly to the $\tilde{A}\,^2B_2$ electronic state, which is strongly coupled with the ground electronic state and undergoes fast predissociation into $NO(\tilde{X}\,^2\Pi)$ and $O(^3P_J, J=0, 1, 2)$. Busch and Wilson [12,13] performed the first measurement of the angular distribution of the O atoms at 347.1 nm by using a molecular beam/time-of-flight technique. Zacharias et al. [14] measured the NO product state distribution

[1] JSPS research fellow.
[2] Present address: Department of Chemistry and Biochemistry, California State University, Fullerton, CA 92634-9480, USA.

following 337 nm dissociation. Internal state and angular distributions of NO fragments were also measured by Mons and Dimicoli [15–17] for several different dissociation wavelengths using one-dimensional time-of-flight mass spectrometry. Recently, the photofragment excitation (PHOFEX) spectra were reported in the near threshold region by monitoring either NO [18] or oxygen atom [19]. In the present study, we apply the imaging technique to the 355 nm photodissociation of NO_2 in the supersonic beam and determine the angular and speed distributions of the NO fragment. The observed angular distribution is compared with the previous reports measured using effusive beams, and the role of rotation of the parent molecule is discussed.

2. Experimental

The experimental apparatus will be described in detail elsewhere [20]. A pulsed molecular beam (5% NO_2: 5% O_2: He at a backing pressure of 2.3 atm) is collimated into a diameter of less than 2 mm and crossed by the pulsed radiation from two lasers. The first is a frequency-tripled Nd:YAG laser (Quanta-Ray, 20 mJ/pulse at 355 nm). The second is a frequency doubled (β-$BaBO_3$) XeCl-pumped dye laser (Lambda Physik EMG 101 and FL2002, 0.5–1.0 mJ/pulse at $\approx$226 nm). The first laser is used to dissociate the NO_2 molecules, while the second, delayed by 50–100 ns, is used to ionize the NO($\tilde{X}\,^2\Pi$) fragment in a selected rovibrational state using (1+1) REMPI through the $\tilde{A}$ state. An electric field of 100–500 V/cm is applied to extract the ion cloud into a Wiley–McLaren time-of-flight (TOF) mass spectrometer [21] placed perpendicular to the plane defined by the laser and molecular beam. The extraction and acceleration voltages are adjusted to flatten the ion cloud into a "pancake" shape just as it hits the microchannel (MCP) detector.

The MCP consists of two plates of 12 μm diameter channels separated by 15 μm (center-to-center) and produces a gain of 8×10^6. Behind each point where an ion strikes the detector, the amplified electrons are accelerated onto the end of a fiberoptic bundle, which is coated with a fast phosphor (P47, 80 ns response). The bundle is fed through a flange in the vacuum chamber, and the image, now a two-dimensional projection of the three-dimensional spatial distribution, is photographed with a 512×480 CID camera equipped with a gated intensifier timed to capture the mass of interest. Finally, the electronic images are sent to a computer averager system. Typically, the NO data images are accumulated for 2^{11}(2048) laser shots, and then a background image caused by the probe laser alone is accumulated for the same number of shots and subtracted from the NO data image. The probe laser generates the weak background image by one-color dissociation/ionization of NO_2 and also by ionizing residual NO impurity in the sample gas.

3. Results

An image of NO($v''=0$, $J''=25\frac{1}{2}$) is shown in fig. 1 as a density plot where the darkest areas correspond to the most intense signal. The image consists of 512×480 pixels and the entire image is approximately 37 mm by 34 mm. The flight time is adjusted to 14.4 μs by varying the repeller voltage, thus optimizing the resolution by making the image as large as possible. In fig. 1, the molecular beam travels from bottom to top, the pump beam enters from the right, and the probe beam enters from the left. Both of the lasers are polarized horizontally in the

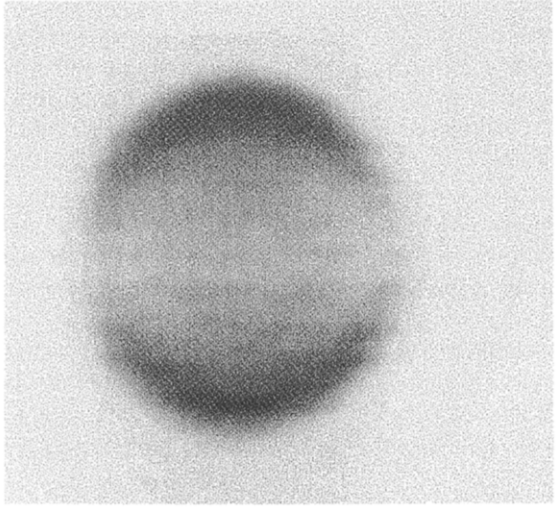

Fig. 1. Image of NO($v''=0$, $J''=25\frac{1}{2}$). The darker areas correspond to a higher density of fragments.

plane formed by their intersection with the molecular beam. Thus, the axis of cylindrical symmetry caused by their polarization vectors corresponds to the vertical center line of the NO image in fig. 1.

Since we know both the position of each ion on the screen and the flight time of the ions from the dissociation laser pulse, the two-dimensional spatial projection is easily converted to a two-dimensional velocity projection. When the projection has been made in a direction perpendicular to an axis of cylindrical symmetry it is possible to reconstruct the full three-dimensional velocity distribution from one two-dimensional projection using an Abel transform [22,23]. Since the three-dimensional velocity distribution is axisymmetric, every planar slice containing the symmetry axis is equivalent, and can be represented as a two-dimensional function of $v_{\parallel}$ and $v_{\perp}$, the velocity parallel to and perpendicular to the polarization of the dissociation laser beam, respectively. This function, $P(v_{\parallel}, v_{\perp})$, is shown in fig. 2. By integrating over all angles at constant speeds the speed distribution, $P(v)$, obtained as shown in fig. 3, where $v=(v_{\parallel}^2+v_{\perp}^2)^{1/2}$ is the speed of the NO. By integrating over all speeds at constant angles the angular distribution, $P(\theta)$, shown in fig. 4 is obtained, where $\theta=\tan^{-1}(v_{\perp}/v_{\parallel})$ is the angle between the polarization of the dissociation laser and the recoil velocity of the NO.

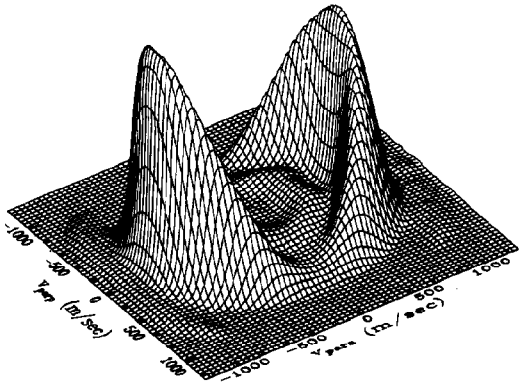

Fig. 2. Abel transform of the image in fig. 1 showing a slice of the three-dimensional distribution. The x- and y-axes correspond to velocity parallel to and perpendicular to the pump laser polarization, respectively. The height is proportional to the number of fragments at the given velocity.

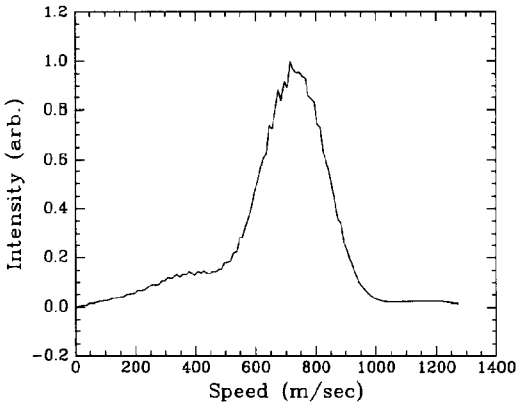

Fig. 3. Speed distribution of NO($v''=0$, $J''=25\frac{1}{2}$), obtained by integrating over all the angles in the distribution shown in fig. 2.

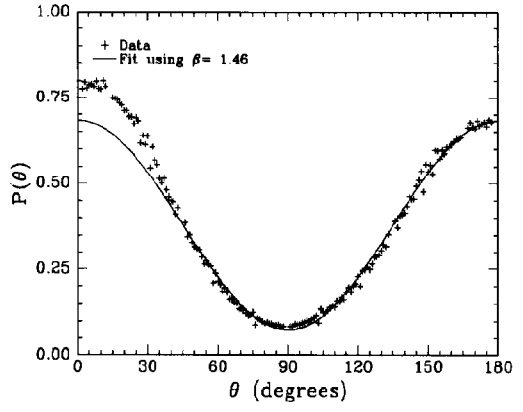

Fig. 4. Angular distribution of NO($v''=0$, $J''=25\frac{1}{2}$). The symbols correspond to the distribution obtained by integrating over all the speeds in fig. 2. The solid line is a fit to the data of the functional form given in eq. (1).

4. Discussion

Following dissociation at 355 nm, NO and O can only be formed in their ground electronic states NO($\tilde{X}\,^2\Pi$) and O(^3P_J, $J=0, 1, 2$), respectively. Due to conservation of energy, therefore, disregarding the spin–orbit splitting of the oxygen atom, only a single speed is allowed for an NO fragment in a given rovibrational state. For NO($v''=0, J''=25\frac{1}{2}$) this speed is 729 m/s, which corresponds to the peak of the observed distribution in fig. 3. The spread in the observed distribution can be attributed to the fact that

the NO fragments do not originate from a point source, but instead they are formed within a volume defined by the overlap of the lasers with the molecular beam.

The angular distribution of photofragments has been considered in detail by many authors [13,24–26]. Typically, the photofragment distributions are characterized by the laboratory frame anisotropy parameter, β, in the equation

$$I(\theta)=[1+\beta P_2(\cos\theta)]/4\pi\,, \qquad (1)$$

where θ is the recoil angle relative to the polarization vector of the photolysis laser and $P_2(x)$ is the second-order Legendre polynomial. For instantaneous dissociation of a diatomic molecule, the anisotropy parameter is -1 for dissociation perpendicular to the transition dipole, μ, or 2 for dissociation parallel to μ. In general, since the dissociation takes place on a finite time scale and since in the dissociation of polyatomic molecules the recoil velocity can have some angle which is neither parallel nor perpendicular to the transition dipole, the measured β actually falls between these two extremes. The functional form given in eq. (1) is fit to the angular distribution of NO($v''=0$, $J=25\frac{1}{2}$) given in fig. 4 in order to determine a value for β of 1.46 ± 0.20. The angular distribution was measured for several other rotational states of NO($v''=0$) and all yielded very similar values of β. Averaging these, we find that $\beta=1.40\pm0.20$.

This value does not agree favorably with previous results of Busch and Wilson [13], who found $\beta=0.74$ ($\lambda_{\rm diss}=347$ nm), nor with the values of $\beta=0.9$ ($\lambda_{\rm diss}=360$ nm) or $\beta=0.6$ ($\lambda_{\rm diss}=348$ nm) reported by Mons and Dimicoli [15,17]. However, the discrepancy can be explained by the effect of rotation of the parent molecule. Neglecting the (small) effect of tangential velocity due to parent rotation, the dependence of β on parent lifetime may be written as [13,25]

$$\beta=2P_2(\cos\chi)\left(\frac{1+\omega^2\tau^2}{1+4\omega^2\tau^2}\right), \qquad (2)$$

where χ is the angle between the parent transition dipole moment and the recoil velocity vector of the fragment, ω is the frequency of the parent rotation, and τ is the lifetime of the parent.

The lifetime of the excited state, τ, is set to 2.1×10^{-13} s by using the data of Busch and Wilson. The rotational frequency can be determined from

$$\tfrac{1}{2}I\omega^2=\tfrac{1}{2}kT\,, \qquad (3)$$

where the average of the two large and nearly equal moments of inertia is used for I, and the temperature of our beam is estimated to be less than 30 K. The dissociation of NO_2 at 355 nm has been shown by Busch and Wilson and by Mons and Dimicoli to be consistent with a transition to the $^2B_2$ state. Since the ground state is totally symmetric, the transition dipole will have the same symmetry as the excited state. This means that the transition dipole moment will be perpendicular to the C_2 axis and in the plane of the molecule. Thus, under the assumption that the oxygen atom leaves along the breaking N–O bond, 2χ is given as 180° minus the bond angle. Assuming that the bond angle is that of the ground state (134°) provides a value of $\chi=23°$, while assuming that bond angle is that of the $^2B_2$ excited state (102°) provides a value of $\chi=39°$ [27]. It is reasonable to assume that the actual recoil angle lies somewhere between these limits. From eq. (2) with the value of τ from Busch and Wilson and a temperature of 30 K, we calculate the expected value of β to lie between 1.0 and 1.5, in agreement with our experimental value. Using this same model and a temperature of 300 K, a value of $\beta\approx0.8$ is obtained, which is close to the values obtained by Mons and Dimicoli and by Busch and Wilson for thermal beams.

One potential problem to consider in the measurements of β using the imaging technique is that the Doppler width of the fragments may be larger than the bandwidth of the probe laser. If this were the case, fragments recoiling along the probe laser propagation direction would be subject to a large Doppler shift and would be only weakly ionized compared to those absorbing in the center of the Doppler profile, where the laser intensity is strongest. In our geometry, where the lasers are counter-propagating, this effect would lead to an increase in the apparent value for β. Given a speed for the NO($v''=0$, $J''=25\frac{1}{2}$) fragment of 729 m/s and an estimated bandwidth at 226 nm of 0.3 cm^{-1} fwhm, the fragments moving directly toward and away from the probe laser will absorb approximately 20% less light. If we assume that the (1+1) REMPI efficiency of NO is linear in laser power, the apparent increment of β by this Doppler effect is calculated to

be less than 0.1 in our experiment, which is somewhat smaller than our experimental error.

Care must also be taken to insure that the entire fragment sphere lies within the cross section of the probe laser at the chosen delay time, otherwise the fragments moving perpendicular to the laser might not be ionized. Such an effect would lower the apparent anisotropy and might occur if both the pump and probe beams are very tightly focused and the time delay between them is large. In our experiment the time delay is only 50–100 ns and the pump beam is not as tightly focused as the probe beam, so that we probe fragments moving in all directions with nearly equal efficiency.

Finally, one must also consider the fact that the photofragments may be rotationally aligned with respect to the relative velocity vector. Because of this so-called v–J correlation, the measured value of β may not reflect the true translational anisotropy, since the detection efficiency of the fragment may depend on the relative orientation of the photofragment with respect to the polarization vector of the probe laser. This effect should be particularly marked in the case of the photodissociation of a cold triatomic molecule, where $v \perp J$ correlation is expected. Although we have investigated the possibility of such an effect, we observe no distinguishable difference between images taken with the probe laser polarized parallel to the pump polarization, as in fig. 1, and images taken with the probe laser polarized perpendicular to the pump polarization. We believe the reason for this is the large cross section of the $\tilde{A} \leftarrow \tilde{X}$ transition, which easily leads to saturation at even moderate laser powers [28]. We have also measured the anisotropy of the O atoms and obtain a β value which is, within experimental error, equal to the NO value, indicating that the measurement is not affected by v–J correlation. Data on the O atom distributions will be described in a more extensive report of the NO_2 photodissociation [20].

5. Conclusion

By applying the technique to the NO_2 dissociation at 355 nm, we have demonstrated that photofragment imaging can be used as a quantitative measure of the dynamics of photodissociations. The anisotropy parameter, β, of a state-selected NO fragment is measured to be 1.40 ± 0.20. Although this is a higher β than reported previously by others workers, it is consistent with a simple model which takes into account the effect of parent rotation. Since the parent is prepared in a colder rotational distribution in our experiment than in previous ones, the value of β we obtain is closer to the limit imposed by the location of the transition dipole moment and the direction of axial recoil. The major advantages of the imaging technique are that the qualitative representation of the data is immediately apparent and that the velocity distribution can be obtained for a state-selected product. Competing product channels can be easily distinguished, thereby reducing the complexity of the quantitative analysis. This technique is therefore suitable to complex dissociations as well as bimolecular reactions.

Acknowledgement

We are grateful to the US Army Research Office for support under grant DAAL03-91-G-0125, to the Science and Engineering Research Council for the award of an Advanced Research Fellowship to BJW, to NATO for the award of a Collaborative Travel Grant to BJW and PLH, and to the Japan Society for the Promotion of Science for the research fellowship to TS. We would also like to thank Dr. D.S. King for his suggestion concerning the effect of the laser linewidth. Dr. Gus Hancock for his suggestion regarding the role of parent rotation, Dr. C.E.M. Strauss for his help in developing the analysis of projection data, and L. Bontuyan for her experimental assistance.

References

[1] D.W. Chandler and P.L. Houston, J. Chem. Phys. 87 (1987) 1445.
[2] R. Schmiedl, H. Dugan, W. Meier and K.H. Welge, Z. Physik A 304 (1982) 137.
[3] R. Ogorzalek Loo, G.E. Hall, H.-P. Haerri and P.L. Houston, J. Phys. Chem. 92 (1988) 5.
[4] R. Ogorzalek Loo, H.-P. Haerri, G.E. Hall and P.L. Houston, J. Chem. Phys. 90 (1989) 4222.
[5] D.W. Chandler, J.W. Thoman Jr., M.H.M. Janssen and D.H. Parker, Chem. Phys. Letters 156 (1989) 151.

[6] D.W. Chandler, M.H.M. Janssen, S. Stolte, R.N. Strickland, J.W. Thoman Jr. and D.H. Parker, J. Phys. Chem. 94 (1990) 4839.
[7] J.W. Thoman Jr., D.W. Chandler, D.H. Parker and M.H.M. Janssen, Laser Chem. 9 (1988) 27.
[8] D.P. Baldwin, M.A. Buntine and D.W. Chandler, J. Chem. Phys. 93 (1990) 6578.
[9] M.A. Buntine, D.P. Baldwin and D.W. Chandler, J. Chem. Phys. 94 (1991) 4672.
[10] C.W. Walter, K.A. Smith and F.B. Dunning, J. Chem. Phys. 90 (1989) 1652.
[11] J. Solomon, J. Chem. Phys. 47 (1967) 889.
[12] G.E. Busch and K.R. Wilson, J. Chem. Phys. 56 (1972) 3626.
[13] G.E. Busch and K.R. Wilson, J. Chem. Phys. 56 (1972) 3638.
[14] H. Zacharias, M. Geilhaupt, K. Meier and K.H. Welge, J. Chem. Phys. 74 (1981) 218.
[15] M. Mons and I. Dimicoli, Chem. Phys. Letters 131 (1986) 298.
[16] M. Mons and I. Dimicoli, Chem. Phys. 130 (1989) 307.
[17] M. Mons and I. Dimicoli, J. Chem. Phys. 90 (1989) 4037.
[18] U. Robra, H. Zacharias and K.H. Welge, Z. Physik D 16 (1990) 175.
[19] J. Miyawaki, K. Yamanouchi and S. Tsuchiya, Chem. Phys. Letters 180 (1991) 287.
[20] V.P. Hradil, T. Suzuki, B.J. Whitaker and P.L. Houston, in preparation.
[21] W.C. Wiley and I.H. McLaren, Rev. Sci. Instr. 26 (1955) 1150.
[22] K.R. Castleman, Digital image processing (Prentice Hall, Englewood Cliffs, 1979).
[23] R.N. Strickland and D.W. Chandler, Appl. Opt. 30 (1991) 1811.
[24] R.N. Zare and D.R. Herschbach, Proc. IEEE 51 (1963) 173.
[25] C. Jonah, J. Chem. Phys. 55 (1971) 1915.
[26] R. Bersohn and S.H. Lin, Advan. Chem. Phys. 16 (1969) 67.
[27] G.D. Gillispie, A.U. Khan, A.C. Wahl, R.P. Hosteny and M. Krauss, J. Chem. Phys. 63 (1975) 3425.
[28] D.C. Jacobs, R.J. Madix and R.N. Zare, J. Chem. Phys. 85 (1986) 5469.